Nanofabrication of Planar Model Catalysts by Colloidal Lithography: Pt/Ceria and Pt/Alumina

ARTICLE *in* LANGMUIR · NOVEMBER 2002

Impact Factor: 4.46 · DOI: 10.1021/la026459j

3 AUTHORS, INCLUDING:

Lars Osterlund
Uppsala University
88 PUBLICATIONS **1,640** CITATIONS
SEE PROFILE

Bengt Herbert Kasemo
Chalmers University of Technology
497 PUBLICATIONS **23,230** CITATIONS
SEE PROFILE

Nanofabrication of Planar Model Catalysts by Colloidal Lithography: Pt/Ceria and Pt/Alumina

Christian Werdinius, Lars Österlund,* and Bengt Kasemo

Department of Applied Physics, and Competence Centre for Catalysis, Chalmers University of Technology, SE-412 96 Göteborg, Sweden

Received August 23, 2002. In Final Form: October 21, 2002

We present a novel method, called colloidal lithography, to prepare well-defined model catalysts on planar supports. The method facilitates fabrication of monodisperse catalyst particles with variable, well-defined size, shape, and interparticle distance. The chemical and structural composition of the constituents (i.e., catalyst particles and support materials) may be independently varied. Large batches of model catalysts may be made in short processing times, with the dimensions of the samples only limited by the physical dimension of available support material, the processing vacuum systems, and so forth. Here we employed 2 in. Si wafers cut into 1×1 cm^2 pieces as the primary lithography support, onto which the support (ceria and alumina) and active catalyst materials (Pt in this case) were deposited. A detailed chemical and structural characterization is presented of the individual steps in the fabrication process. The oxygen plasma used to remove the colloidal mask residues is shown to lead to substantial but reversible Pt oxidation. As a probe reaction, to validate the nanofabrication process, CO oxidation measurements were performed on 130 nm Pt particles on an alumina or a ceria support. The reactivity measurements are in good agreement with literature data and suggest a satisfactory performance of the colloidal lithography model catalysts.

1. Introduction

The physical and chemical properties of nanometer-sized structures have gained increasing interest during the past decade. This is mainly due to the continued striving for miniaturization in microelectronics, but also motivated by many applications in other R&D areas, such as nonlinear optics,[1] (bio)sensors,[2] protein adsorption,[3] and catalysis.[4] In the area of heterogeneous catalysis, it has been shown that intrinsically new phenomena may occur on the nanometer scale, which cannot be deduced from the knowledge obtained from extended surface of bulk phenomena. This is due to changes in the electronic structure, morphology, and kinetics of nanometer scale particles.[5−7] These advancements stem in part from the development of analytical tools which enable detailed investigations of the properties of small supported catalysts[7] but also from development of methods and techniques to synthesize well-controlled model systems at the nanometer scale.[8−13]

In heterogeneous catalysis, the catalysts often consist of catalytically active components of noble metals such as Pt, Rh, and Pd, supported on an oxide support, which serve several tasks, for example, to stabilize the noble metal particles toward sintering, to maintain a high dispersion, and to act as a reservoir to intermittently store or release compounds, that is, to actively take part in the overall catalyst reaction.[14] Very little quantitative information is, however, available for this latter function. A common way of making such catalysts is by wet-impregnation.[15] This technique is effective for making catalysts with a high specific surface area, which is very important for commercial applications where high throughput and low price are required. It yields, however, a complex 3D catalyst structure, with a heterogeneous size distribution of the noble metal and support particles. Attempts to make well-defined model catalysts include for example vapor deposition[5,16,17] and cluster source methods,[8] which allow controlled preparation in vacuo. In terms of simultaneous control of particle size, interparticle separation, and component interaction, electron-beam lithography is probably superior to most other techniques.[9,10] It is a valuable method for research, but it is an expensive technique, and making large areas (∼cm^2) with small features is very time consuming and costly. Additionally it has a lower limit regarding how small the particles can be made (a limit which is continually improving). Other methods include spin-coating[13] and the use of metal-loaded block copolymer micelles.[11,18] A common problem that arises when employing ex situ methods for model catalyst fabrication is the issue of chemical cleanliness, which is accentuated by

* Corresponding author. E-mail: lars.osterlund@fy.chalmers.se.

(1) Joannopoulos, J. D.; Villeneuve, P. R.; Fan, S. H. *Nature* **1997**, *386*, 143.
(2) Wagner, P.; Spudich, A.; Ulman, N.; Chidsey, C. E. D.; Spudich, J. A. *Biophys. J.* **1997**, *72*, 452.
(3) Denis, F. A.; Hanarp, P.; Sutherland, D. S.; Gold, J.; Mustin, C.; Rouxhet, P. G.; Dufrene, Y. F. *Langmuir* **2002**, *18*, 819.
(4) Kasemo, B.; Johansson, S.; Persson, H.; Thormahlen, P.; Zhdanov, V. P. *Top. Catal.* **2000**, *13*, 43.
(5) Henry, C. R. *Surf. Sci. Rep.* **1998**, *31*, 235.
(6) Zhdanov, V. P.; Kasemo, B. *Surf. Sci. Rep.* **2000**, *39*, 29.
(7) Somorjai, G. A. *Introduction to surface chemistry*; Wiley: New York, 1994.
(8) Heiz, U.; Schneider, W. D. *J. Phys. D* **2000**, *33*, 85.
(9) Jacobs, P. W.; Ribeiro, F. H.; Somorjai, G. A.; Wind, S. *J. Catal. Lett.* **1996**, *37*, 131.
(10) Johansson, S.; Österlund, L.; Kasemo, B. *J. Catal.* **2001**, *201*, 275.
(11) Möller, M.; Spatz, J. P. *Curr. Opin. Colloid Interface Sci.* **1997**, *2*, 177.
(12) Holmberg, K. In *Micelles, Microemulsions and Monolayers*; Shah, D. O., Ed.; Marcel Dekker: New York, 1998.
(13) Vanhardeveld, R. M.; Gunter, P. L. J.; Vanijzendoorn, L. J.; Wieldraaijer, W.; Kuipers, E. W.; Niemantsverdriet, J. W. *Appl. Surf. Sci.* **1995**, *84*, 339.
(14) Trovarelli, A. *Catal. Rev.—Sci. Eng.* **1996**, *38*, 439.
(15) Ertl, G.; Knözinger, H.; Weitkamp, J. *Handbook of Heterogeneous Catalysis*; Wiley−VCH Verlag: Weinheim, Germany, 1997; Vol. 1.
(16) Rainer, D. R.; Xu, C.; Goodman, D. W. *J. Mol. Catal. A: Chem.* **1997**, *119*, 307.
(17) Freund, H. J.; Baumer, M.; Kuhlenbeck, H. *Adv. Catal.* **2000**, *45*, 333.
(18) Spatz, J. P.; Herzog, T.; Mossmer, S.; Ziemann, P.; Moller, M. *Adv. Mater.* **1999**, *11*, 149.

10.1021/la026459j CCC: $25.00
Published on Web 11/23/2002

the use of chemicals for the actual synthesis or for cleaning purposes.

In this paper, we describe a method called colloidal lithography, which utilizes surface chemical techniques for defining a (nano)pattern and lithographic techniques to develop the pattern. Previous attempts to use colloidal particles as masks for lithographic processes have mainly consisted of deposition of metal between particles in close-packed arrays.[19−21] The domains of close-packed particles are of limited size (∼100 μm^2), which results in noncontinuous structures of nanoparticles. Here we instead allow the colloidal particles to self-assemble on top of metal films of the active catalyst material and develop the pattern by directed Ar^+ sputtering. Colloidal lithography has previously been used in our group to make nanopatterned surfaces for biomaterials applications.[3,22] Here we extend these results and demonstrate new steps in the preparation procedures to achieve 3D architecture. In particular, we show that we can fabricate chemically well-controlled model catalysts by the colloidal lithography technique. Using CO oxidation as a probe reaction, we present results of the catalytic activity on Pt/alumina and Pt/ceria model catalysts.

2. Experimental Section

2.1. Sample Preparation. As the primary substrate in the colloidal lithography processing, we have used 0.37 mm thick 2 in. Si(100) wafers with a thermally grown SiO_2 layer, 1000 or 3000 Å thick; the former thickness was used in the temperature-programmed desorption (TPD) measurements. This choice is made for practical reasons: (i) The Si wafers are atomically smooth (i.e., determined only by the intrinsic step density distribution) and therefore do not introduce additional surface roughness. This is in principle no strict requirement, but it simplifies the process analysis. (ii) The Si wafer is readily available atomically flat up to very large dimensions, which we make use of here. (iii) Oxidized Si wafers are chemically and physically well characterized, and the SiO_2 termination provides a barrier for Si intermixing into films evaporated onto the silica surface.

The wafers were cut into 1 × 1 cm^2 pieces with a diamond saw (Loadpoint Microace 3+), either prior to or after the colloidal lithography process. Support films, 20−50 nm thick, of either alumina or ceria were deposited onto the substrate (1−2 Å/s) in a sputter/evaporation chamber (AVAC HVC-600), by e-beam evaporation of pressed tablets made from powder of aluminum oxide (Kebolab) and cerium(IV) oxide (Alfa, 99.9%). The thickness of the deposited film was measured with a quartz crystal microbalance (QCM) crystal and calibrated by independent profilometer (Tencor Alpha Step 500) measurements. Platinum (KA Rasmussen, 99.95%) films, 20−100 nm thick, were evaporated onto the support with the same technique. The surfaces were treated with a water solution of 10 w/w (w/w = weight percentage) aluminum chloride hydroxide (ACH, Reheis) to make them positively charged. In some cases, the surfaces were treated with 2 w/w poly(diallyldimethylammonium) (PDDA, MW 200 000−350 000, Aldrich) and 2 w/w poly(sodium 4-styrenesulfonate) (PSS, MW 70 000, Aldrich) before the ACH treatment. For the colloidal particle adsorption, water suspensions of 0.1 w/w negatively charged sulfate-terminated polystyrene (PS) particles (Interfacial Dynamics Corp.) with a diameter of 107 or 41 nm, respectively, were used with 0−10 mM added sodium chloride (NaCl, Merck, pro analysis). Anisotropic ion etching was performed on a rotating sample by directed Ar^+ bombardment (sputtering) (Oxford CAIBE Ion Beam System) with normal incidence at a beam energy of 500 V, resulting in a sample current of 0.2 mA/cm^2. Radio frequency induced, low-temperature oxygen plasma (Plasma Therm PE/RIE m/95) was used to remove the PS particles (250 W, 500 mTorr, 2 min). Some samples were subsequently reduced in hydrogen plasma (250 W, 500 mTorr, 2 min). Oxygen plasma was also used to clean the Si substrate before the evaporation steps and also before adsorption of the PS particles (50 W, 250 mTorr, 2 min). All the steps in the colloidal lithography process were performed in a clean room environment (class 1000 or class 10000) at the Microtechnology Centre at Chalmers (MC2).

2.2. Characterization. Structural characterization of the samples was done by scanning electron microscopy (SEM, JEOL JSM-6301F) and by atomic force microscopy (AFM, Digital Instruments Nanoscope III). The SEM pictures were analyzed with the software package Scion Image from Scion Image Corp.

Chemical analysis was done by X-ray photoelectron spectroscopy (XPS, Perkin-Elmer PHI 5000C ESCA system), employing 400 W Mg Kα radiation, with the detector placed at 45° with respect to the surface. The binding energy calibration was done by internal calibration against the C1s peaks. Curve deconvolution was performed with the software package MultiPak V6.0A (Physical Electronics, Inc.). A pretreatment system, equipped with a separate gas-handling system, attached to the XPS system, allowed for in situ sample transfer between each cycle of pretreatment (up to atmospheric pressures) and XPS analysis. Secondary ion mass spectrometry (SIMS) measurements were done on a Cameca IMS 3F instrument employing O^{2+} ions at 2 kV at a 70° angle of incidence.

The CO oxidation measurements were performed in a flow reactor (30 cm^3/min), with an interior volume of 6 cm^3. The thin (∼0.3 mm) samples with dimensions of 1 × 1 cm^2 were mounted in the flow reactor by pressing a spring-loaded thermocouple against the front sample surface. The samples were heated from the back side by IR heating through a quartz window onto which the sample was placed. The outlet gas composition was analyzed by feeding the gas through a quartz capillary leak, positioned ∼1 mm above the sample surface, via a directed gas inlet tubing into a cross beam ion source of a quadrupole mass spectrometer (Balzers).[23] The mass spectrometer signal was converted to a total conversion yield (%), using the calibrated CO_2 cracking pattern to obtain the correct CO content at $m/Z = 28$. All CO oxidation experiments were performed in oxygen excess using a gas mixture of 0.3% CO and 1.2% O_2 diluted in Ar, unless otherwise stated, and employing a linear heating ramp of 10 K/min.

3. Results and Discussion

3.1. Process Description. The basic idea of colloidal lithography, as used here, is to combine the advantages of the lithographic methods, in terms of processing purity and versatility, and colloidal chemical methods in terms of self-assembling properties, process speed, and cost-effectiveness (Figure 1, left column). At the heart of the process lies the idea of creating a colloidal mask with the desired properties (chemical composition, size, shape, charge, etc.), which can be used to shield the surface beneath the colloidal particles during the etching (Figure 1, steps I and II) and which can subsequently be removed to expose the underlying (masked) surface (Figure 1, step III). One of the benefits with colloidal lithography is the possibility to process large areas in a short processing time. A general comment should be made on the particle size right at the start, since the general interest in catalysis typically is particles of <20 nm in diameter: While there are inherent problems with producing very small (a few nanometers in diameter) particles by colloidal lithography, which we describe below, the main reason for making fairly large particles (107 nm) in the present study is the ease by which they can be analyzed with SEM and AFM compared to smaller particles. Each step of the process is

(19) Boneberg, J.; Burmeister, F.; Schafle, C.; Leiderer, P.; Reim, D.; Fery, A.; Herminghaus, S. *Langmuir* **1997**, *13*, 7080.
(20) Hulteen, J. C.; Treichel, D. A.; Smith, M. T.; Duval, M. L.; Jensen, T. R.; Van Duyne, R. P. *J. Phys. Chem. B* **1999**, *103*, 3854.
(21) Burmeister, F.; Badowsky, W.; Braun, T.; Wieprich, S.; Boneberg, J.; Leiderer, P. *Appl. Surf. Sci.* **1999**, *145*, 461.
(22) Hanarp, P.; Sutherland, D.; Gold, J.; Kasemo, B. *Nanostruct. Mater.* **1999**, *12*, 429.
(23) Kasemo, B. *Rev. Sci. Instrum.* **1979**, *50*, 1602.

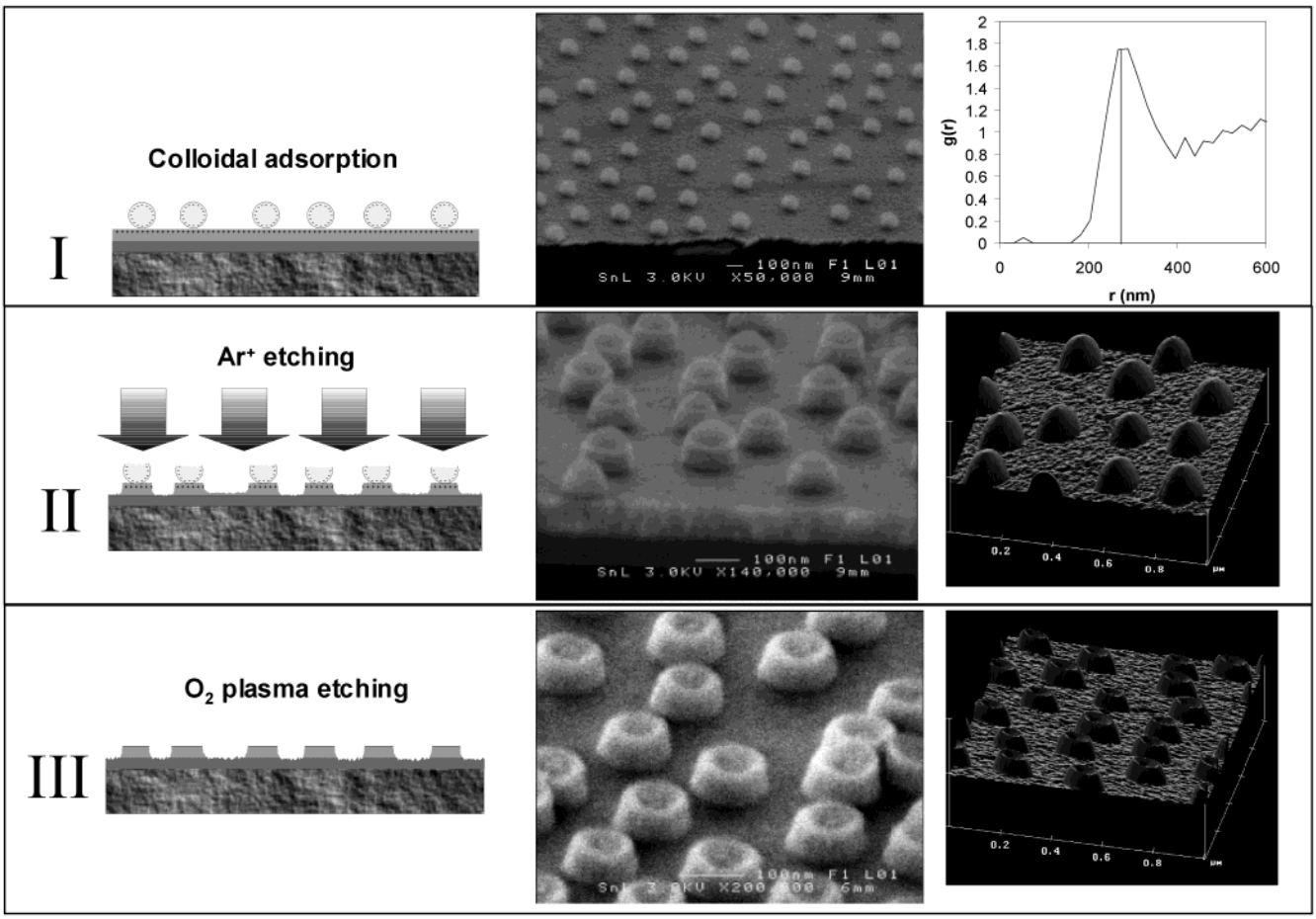

Figure 1. The basic colloidal lithography fabrication steps (left panel) to make supported Pt model catalysts, with the corresponding SEM (middle panel) and AFM (right panel) images of a Pt/ceria model catalyst. On the top right the RDF of the initial PS/Pt/ceria sample is shown.

demonstrated in Figure 1 by the fabrication of Pt dots on a ceria support by using 107 nm PS particles as template. In the following sections, we will describe each process step in more detail.

I. A 50 nm thick ceria film is evaporated on a thermally oxidized Si wafer. A 30 nm thick Pt film is subsequently evaporated on top of the ceria film. A solution of 10 w/w ACH is put on the Pt surface with a pipet to give it a positive charge, which originates from aluminum ions (Al^{3+}) adsorbed on the surface, as demonstrated by XPS measurements. After 30 s, the surface is rinsed in water and blown dry with nitrogen gas. A water suspension of 0.1 w/w 107 nm PS particles is then rapidly poured over the Pt surface to immediately cover the whole surface with the colloidal suspension. After 5 min, the sample is again rinsed in water and blown dry with nitrogen gas. The negatively charged PS particles adsorb on the positively charged Pt surface in a hit and stick manner. Electrostatic repulsion, however, prevents them from adsorbing closer to a neighboring particle than a certain minimum distance (see section 3.2), which eventually leads to a self-assembled monolayer of adsorbed colloidal particles. The colloidal adsorption is qualitatively well described by a modified random sequential adsorption (RSA) model.[24] The colloids only have short-range order. The nearest-neighbor distance is well-defined as seen in the radial distribution function (RDF) plot[25] (Figure 1), which exhibits a clear peak (defining the nearest-neighbor distance).

II. The surface is etched by directed Ar^+ sputtering (4 min, 500 V, 0.2 mA/cm^2), which removes the Pt (etch rate, 13 nm/min) not shadowed by adsorbed PS particles. The etching is continued 10 nm into the ceria layer (etch rate, 6 nm/min) to ensure that all of the exposed Pt is removed.

III. The PS particles are removed by an O_2 plasma treatment (250 W, 500 mTorr, 2 min). In section 3.7 below, we present XPS results, which describe the effect of oxygen plasma treatment regarding removal of the PS particles and also regarding the accompanying oxidation of Pt. It is not possible to dissolve the PS particles in for example acetone after the Ar^+ etching process, which may be due to ion-induced cross-linking of the polymer chains during the ion etching.[25,27]

3.2. Interparticle Separation. As described above, the closest allowed distance between adsorbed colloidal PS particles is determined by electrostatic repulsion, described in more detail by the Derjaguin−Landau−Verwey−Overbeek (DLVO) theory.[28] When salt is added to the colloidal suspension, the interparticle repulsion is weakened by electric double layer screening (decrease of the reciprocal Debye length), and the particles may adsorb closer to each other.[29,30] Figure 2 shows Pt dots on a ceria support using 107 nm PS particles as templates and NaCl

(24) Adamczyk, Z.; Zembala, M.; Siwek, B.; Warszynski, P. *J. Colloid Interface Sci.* **1990**, *140*, 123.

(25) Sjollema, J.; Busscher, H. J. *Colloids Surf.* **1990**, *47*, 337.

(26) Netcheva, S.; Bertrand, P. *J. Polym. Sci., Polym. Phys.* **2001**, *39*, 314.

(27) Bouffard, S.; Balanzat, E.; Leroy, C.; Busnel, J. P.; Guevelou, G. *Nucl. Instrum. Methods B* **1997**, *131*, 79.

(28) Garbassi, F.; Morra, M.; Occhiello, E. *Polymer Surfaces: From Physics to Technology*, 2nd ed.; John Wiley & Sons: New York, 1998.

(29) Johnson, C. A.; Lenhoff, A. M. *J. Colloid Interface Sci.* **1996**, *179*, 587.

(30) Semmler, M.; Mann, E. K.; Ricka, J.; Borkovec, M. *Langmuir* **1998**, *14*, 5127.

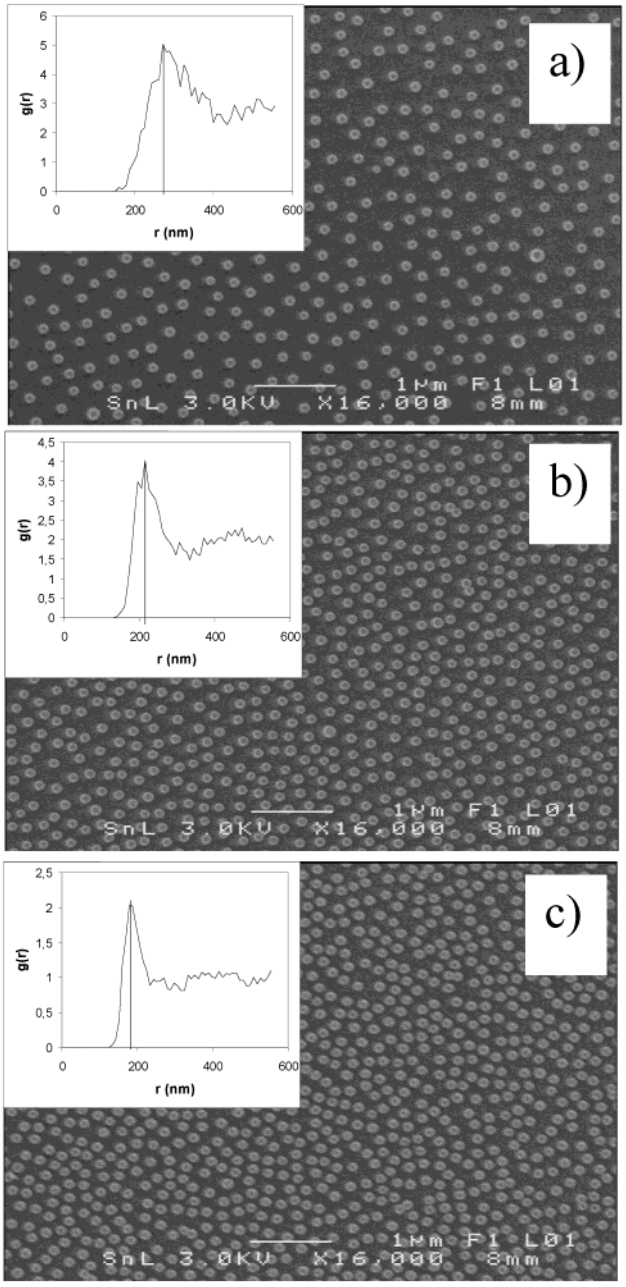

Figure 2. 107 nm Pt/ceria samples made with three different NaCl concentrations, resulting in different surface coverage, projected surface area Pt coverage, and interparticle separation, respectively: (a) 0 mM, 13%, 270 nm (corresponding to Figure 1); (b) 0.5 mM, 27%, 215 nm; (c) 1 mM, 40%, 180 nm. The insets show the RDF with the main peak indicated (corresponding to the nearest-neighbor center-to-center distance).

concentrations between 0 and 1 mM in the suspensions. The insets in Figure 2 show the RDF curve at each salt concentration. The projected geometrical coverage of the Pt dots increases from 13 to 40% (corresponding to a particle density of $3.6 \times 10^{10}/\text{cm}^2$ and $1.1 \times 10^{11}/\text{cm}^2$, respectively) with increasing NaCl concentration in the colloidal suspension. The corresponding decrease of nearest-neighbor distance obtained from the RDF shows a decrease from 270 to 180 nm. The former value (270 nm) corresponds to the largest interparticle distance, which is possible to obtain with 107 nm particles (no salt added). It is difficult to obtain colloids that are more densely packed than those with a 180 nm nearest-neighbor distance in this particular case, due to agglomeration. Note that the RDF from the initial colloidal adsorption step (Figure 1, top right) is preserved throughout the nanofabrication procedure (Figure 2a)

When high salt concentrations (>1 mM NaCl for 107 nm particles) are used in the suspension, making the colloidal particles adsorb close together, the tendency for agglomeration is large. Also, with no added salt the disruption of the ordered pattern of the adsorbed colloids during drying may be a problem for larger particles (>200 nm), which is due to the lower ratio between the attractive forces between the substrate and the particles and the strong lateral forces (see section 3.5) during drying. There are, however, tricks to avoid this.[3] The simplest and most effective way is to dip the sample into boiling water for 30 s after the adsorption of the colloidal PS particles. It is important not to allow the sample surface to dry before the immersion in the hot water bath. The glass transition temperature for PS is about 100 °C, so the boiling water will partly melt the PS particles and glue them to the substrate, which seems to immobilize them and counteract agglomeration. After the boiling step, the sample is again rinsed in water and dried as described above.

3.3. Particle Shape. The SEM and AFM micrographs after the final step in the colloidal lithography process in Figure 1 (step 3) show a craterlike or cuplike shape of the Pt dots. It arises when Pt, which is sputtered away from the surface by argon ions, redeposits underneath the adsorbed PS particles, schematically illustrated in Figure 4a. Figure 4b shows a SEM micrograph of how a Pt cup has started to form around an adsorbed 530 nm PS particle during the Ar^+ etching. If planar Pt dots are desired, the trick is to partially melt the adsorbed PS particles to halfspheres prior to the Ar^+ etching, thus preventing redeposition of Pt (Figure 4c). Figure 4d shows 130 nm flat Pt dots on ceria made by adsorption of 107 nm PS particles (0.2 mM NaCl in the particle suspension), which were melted to hemispheres (2 min at 112 °C on a hot plate), prior to the Ar^+ etching. The melting increases the diameter of the adsorbed particles to 130 nm, which also leads to fusion of some adjacent particles. In the following, we denote Pt particles which have a cuplike structure simply as Pt dots/particles, while those which are made by premelting are denoted "flat" Pt dots/particles.

3.4. Particle Size. The size of nanoparticles resulting from the colloidal lithography process can simply be controlled by using colloidal particles with the desired size. Polystyrene colloids are commercially available in sizes from about 20 nm up to several micrometers. Silica colloids are commercially available with diameters from a few nanometers and upward, which can be made almost monodisperse by autoclave treatments. Figure 3 shows adsorbed PS colloids with diameters of 107 and 41 nm, respectively, as specified by the manufacturer. It is notable that the colloids with 41 nm specified diameter have a significantly broader size distribution than those with 107 nm diameter. This originates primarily from the manufacturing process of the PS colloidal particles, which gives more polydisperse particles at the smaller sizes. The polydispersity is, however, amplified by the adsorption process, as shown by Hanarp et al.,[31] making the size distribution of the adsorbed particles broader and shifted toward smaller diameters compared to the size distribution in the suspension. This is because the small particles diffuse faster in the suspension and also may adsorb between larger particles, where the adsorption of larger particles is prevented. One interesting approach would be to use proteins, which are totally monodisperse, as masking particles in the colloidal lithography process, for

(31) Hanarp, P.; Sutherland, D. S.; Gold, J.; Kasemo, B. *J. Colloid Interface Sci.* **2001**, *241*, 26.

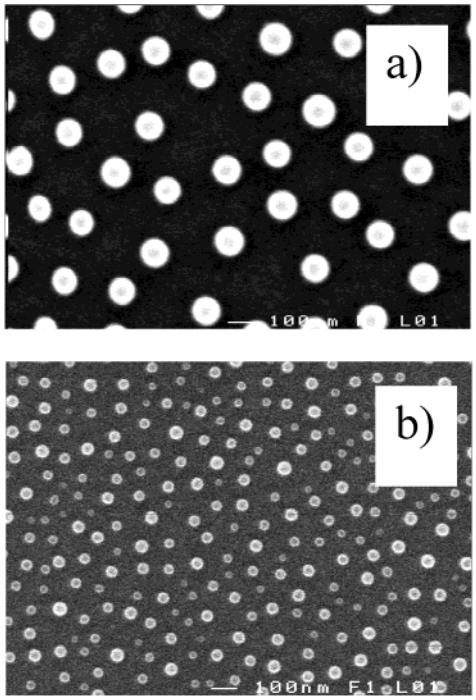

Figure 3. (a) 107 nm and (b) 41 nm polystyrene particles on a Pt film.

example, the spherical iron-containing protein ferritin, with a diameter of about 13 nm.[32]

As mentioned above, the process described so far has a lower limit for the surface coverage (with no added NaCl to the suspension), for example, 13% for 107 nm PS particles (Figure 2a). If lower surface coverages and/or smaller particles are desired, a trick is to adsorb larger particles and shrink them to the desired size using a mild oxygen plasma treatment prior to Ar^+ etching.[33] A more straightforward approach is to use extended Ar^+ etching times, that is, longer times than necessary to etch through the Pt layer, thus etching the PS particles to the desired size, utilizing the fact that the PS is etched at a rate of ~7 nm/min with the parameters employed (500 V, 0.2 mA/cm^2) (Figure 5a).

Figure 5b,c shows 40 nm Pt dots on an alumina support made by the following steps: (i) adsorption of 107 nm PS particles on a 30 nm thick Pt film on 30 nm thick alumina, (ii) melting of the PS particles to "hemispheres" ($T = 112$ °C, 2 min) (see below for a more thorough discussion on the melting), (iii) 6 min Ar^+ etching (etch rate: Pt, ~13 nm/min; alumina, ~3 nm/min), and finally, (iv) removal of the remaining PS with an oxygen plasma treatment. This method causes the underlying (support) material to be etched much more compared to the methods described in section 3.1, since the surfaces are intentionally etched for longer times than required to remove the Pt layer. The elevation in the alumina layer around each Pt dot in Figure 5c indicates the size of the original PS particle. If a continuous support film is desired, it is important to make it thick enough so it is not etched through during the extended Ar^+ etching step, used to shrink the PS particles. On the other hand, the support layer may be intentionally etched through to create multicomponent 3D units (Figure 6a), consisting of an individual catalyst particle on a larger support particle, not physically connected to the support of neighboring particles. Figure 6b shows 70 nm Pt dots on 170 nm ceria islands situated on the bare silica surface.

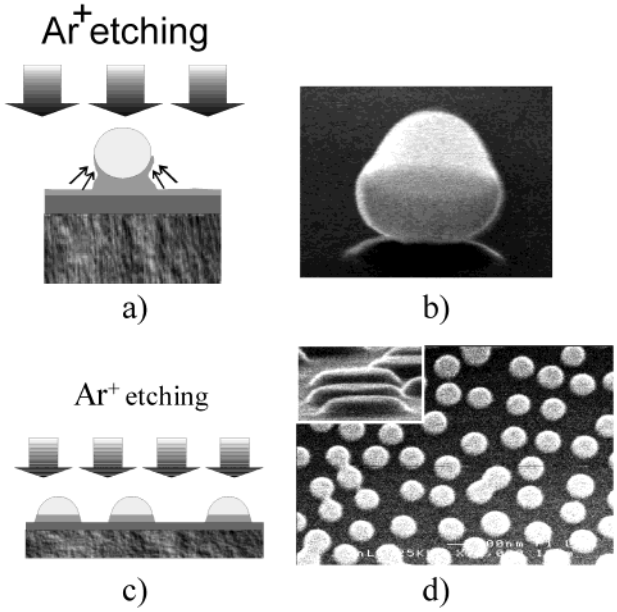

Figure 4. (a) "Cuplike" structures formed from Pt deposited underneath the adsorbed PS particles during Ar^+ etching. (b) SEM micrograph depicting how a Pt cup has started to form around an adsorbed 530 nm PS particle during the Ar^+ etching. (c) By partly melting the adsorbed PS particles to hemispheres prior to the Ar^+ etching, redeposition is avoided and flat Pt dots are formed. (d) SEM micrograph of flat 130 nm Pt/ceria dots, 20 nm high, formed by partly melting 107 nm PS particles prior to Ar^+ etching. The melting leads to an increased particle size (110 nm → 130 nm) and to fusion of some adjacent particles.

The structures were made by the following procedure: (i) adsorption of 200 nm PS particles, which were subsequently melted to hemispheres, on a 30/30 nm Pt/ceria film; (ii) Ar^+ etching for 9 min, that is, significant overetching (the etch rate is ~13 and ~6 nm/min for Pt and ceria, respectively, resulting in ca. 2.7 min etching into the bare silica surface, or ca. 22 nm with an etch rate of 8 nm/min for silica); (iii) removal of the remaining PS by an oxygen plasma treatment.

The different inclinations of the etched Pt, ceria, and silica in Figure 6b and the alumina in Figure 5b originate from their different etch rates. By variation of the size of the adsorbed particles, the degree of melting (thickness of the melted PS particles), the thickness and materials of the evaporated films, and the Ar^+ etching times, many different structures can be made.

3.5. Drying. A critical step during the colloidal lithography process is the drying of the sample, after the adsorption of the PS colloidal particles and the rinsing in water. Failure to control the particle (im)mobility during drying can ruin the whole process. During the drying process, capillary forces act between the adsorbed particles, tending to aggregate them into clusters.[29,34] Larger particles exhibit a higher tendency for agglomeration than smaller ones. Whether the colloidal particles will agglomerate during the drying phase depends on the ratio between the lateral capillary forces and the attractive forces between the colloidal particles and the support. The lateral forces originate from the receding waterfront and the water meniscus, which forms between two adjacent particles during the drying process. The extension of the meniscus is dependent on the contact angle between the water and the surface of the sample. A small contact angle, that is, a hydrophilic sample surface, allows a water meniscus to form between two particles further away from

(32) Feder, J.; Giaever, I. *J. Colloid Interface Sci.* **1980**, *78*, 144.
(33) Haginoya, C.; Ishibashi, M.; Koike, K. *Appl. Phys. Lett.* **1997**, *71*, 2934.
(34) Kralchevsky, P. A.; Nagayama, K. *Langmuir* **1994**, *10*, 23.

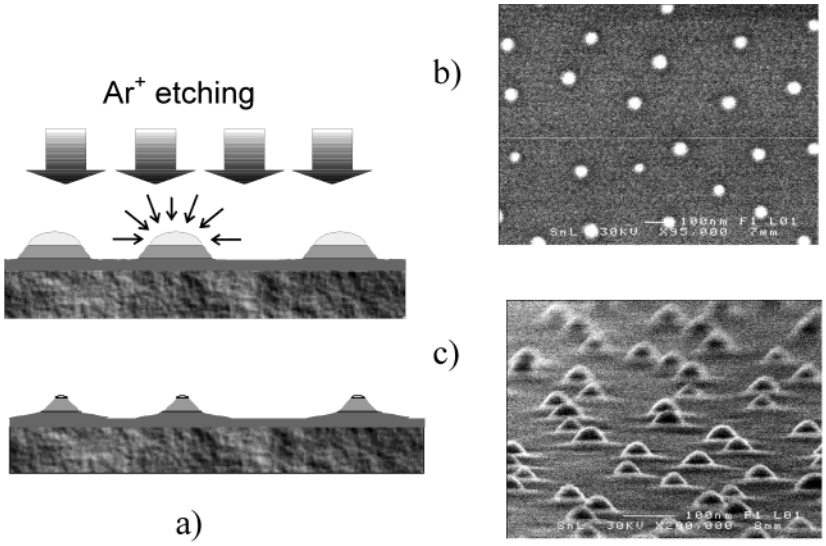

Figure 5. (a) By utilizing extended Ar^+ etching times, the (premelted) PS particles are shrunk during the etching, resulting in smaller PS particles than the original PS mask, which may be used to create low-coverage regimes not accessible by using smaller colloidal particles as templates. (b) SEM micrograph of ~40 nm Pt dots on alumina created from 107 nm PS particles, which were melted to hemispheres and exposed to 6 min Ar^+ etching (2.5 min is enough to etch through the 30 nm thick Pt layer). (c) An inclined view, ~85°, reveals the size of the original PS particle as an elevation in the alumina in a zone around the Pt particles.

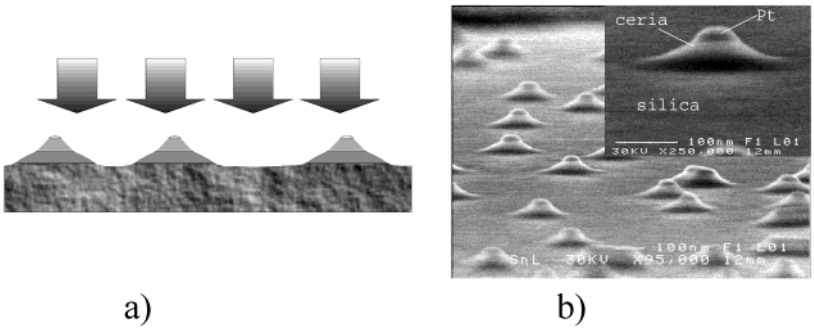

Figure 6. (a) By using extended Ar^+ etching times and continuing the etching through the support layer, it is possible to make 3D multicomponent structures. (b) A SEM micrograph of Pt/ceria/silica structures with 50 nm Pt dots on top of larger ceria particles situated on a silica surface.

each other than if the surface is more hydrophobic, which increases the tendency for particle agglomeration on a more hydrophilic surface. A too hydrophobic surface, on the other hand, prevents the adsorption of aluminum ions during the ACH treatment of the sample surface (step 1 in Figure 1). An optimal contact angle seems to be around 50°. Depending on the choice of material and the pretreatment (e.g., O_2 plasma, which increases the hydrophilicity for most materials), it can be hard to achieve this ideal contact angle. A trick is then to adsorb a double layer of the positive polyion PDDA and the negative polyion PSS as a first step in the colloidal lithography process, before the adsorption of the positive aluminum ions by the ACH treatment. The coating gives the surface a contact angle close to the optimal 50°, independent of which substrate is used. Adsorption of the double layer is simply done by exposing the sample to 2% solutions of PDDA and PSS, for 30 s each. Between and after the adsorption steps, the sample is rinsed in water and blown dry with N_2. After subsequent adsorption of ACH, the thickness of the triple layer PDDA/PSS/ACH is ca. 1 nm.[35]

A common reason for disruption of the ordered colloidal pattern during the drying process is that water re-enters areas that have already been dried. The advancing waterfront may then push the particles away from their adsorption sites (Figure 7a). It is thus very important to blow off the water in a unidirectional, controlled manner. Another reason to blow-dry the samples is that the waterfront affects the particles with less force when it recedes with high speed.[36] This is the reason self-dried samples tend to agglomerate more (Figure 7b) than if the water is forced off the surface with N_2. Preliminary results indicate that another way to dry the sample, without the need for skill in the handling of the nitrogen blow-gun, is to pour methanol on the sample after the final rinsing step in water (to reduce the surface tension) and spin-dry it at 1000 rpm.

3.6. Argon Ion Etching. An important issue in the fabrication process of model catalysts is to make sure that no residue of (catalytically active) material removed during the Ar^+ etching process is embedded in the support. Since Ar^+ sputtering gives rise to a distribution of secondary ions in the impact scattering process, which in turn scatter approximately isotropically around the center of impact, it cannot ad hoc be presumed that no Pt is buried in the ceria during the Ar^+ sputtering process. Dynamic SIMS depth-profiling (Figure 8) of a 30 nm Pt film on ceria with O_2^+ ions (2 kV, 1.2 mA/cm^2) shows, however, that the Pt signal drops sharply under the detection limit (<1000 ppm) when the ceria layer is reached (the sputtering mechanism

(35) Dubas, S. T.; Schlenoff, J. B. *Macromolecules* **1999**, *32*, 8153.

(36) Visser, J. *Part. Sci. Technol.* **1995**, *13*, 169.

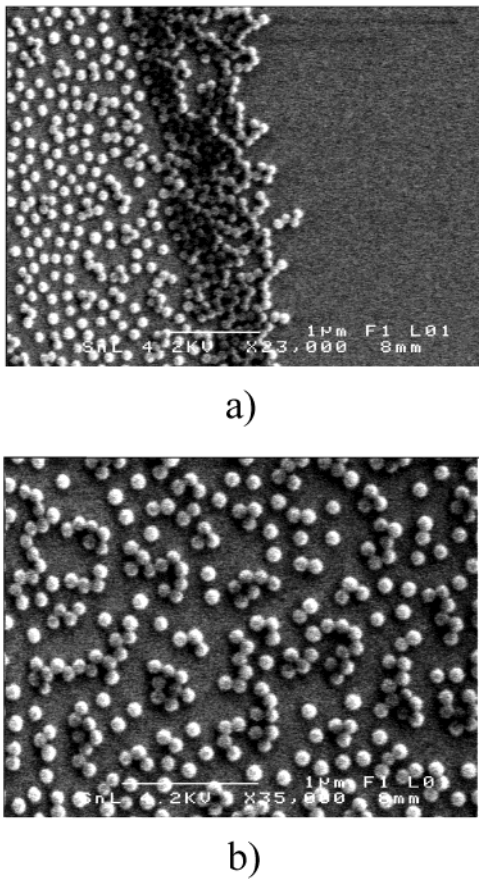

Figure 7. Critical aspects of drying the sample immersed in a PS colloidal suspension. Typical failures: (a) water has re-entered a dried area and pushed away the adsorbed particles on the right part of the picture to a particle front; (b) agglomeration has occurred on a sample slowly dried in air.

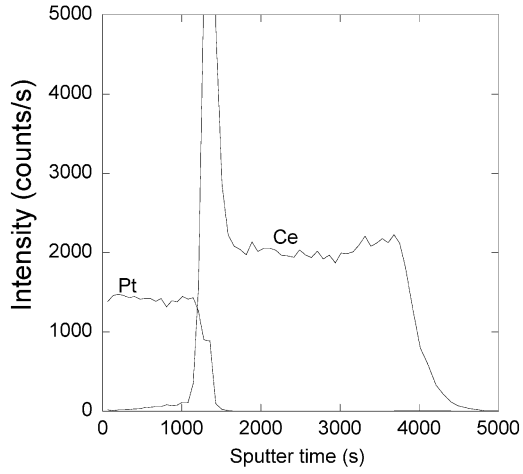

Figure 8. Dynamic SIMS depth profiling of a 30 nm thick Pt film on top of a 50 nm thick ceria film evaporated on an oxidized silicon wafer. The overshoot in the Ce signal is due to a time lag in the automated charge compensation.

with Ar^+ ions and O_2^+ ions is assumed to be essentially the same at these beam energies). These data suggest that no Pt is buried in the ceria layer during the Ar etching process and that the only Pt remaining after etching originates from Pt underneath the PS particles.

3.7. Removal of the Polystyrene Template Particles. An important issue is how to remove the remains of the polystyrene colloidal particles after the Ar^+ etching step. The procedure we have chosen in the present study is to use an O_2 plasma treatment (step 3 in Figure 1). It is important to determine the chemical and structural status of the sample after this final step. While SEM and AFM images reveal only the expected Pt particles, it is necessary to confirm that there are no chemical traces left at all, since submonolayers of PS traces may deteriorate the catalytic activity substantially. Three different sample categories were prepared (by processing precut 2 in. Si wafers, which were snapped into 1 cm^2 pieces after the fabrication process) for XPS analysis:

1. A 100 nm Pt film was evaporated on a Si wafer (coated with 30 nm ceria because of the poor attachment between Pt and silica).

2. An identical Pt film on ceria was prepared and subsequently subjected to all the steps in the colloidal lithography process according to the following procedure: A dense layer (10 mM NaCl in the particle suspension) of 107 nm PS particles was adsorbed and melted to a homogeneous PS film (174 °C, 4 min). The sample was Ar^+ etched for 2.3 min (500 V, 0.2 mA/cm^2). This treatment, which did not etch through the PS film, was included to mimic the Ar^+ treatment when the material not shadowed by the PS was removed. The step was included because of the observed cross-linking of the polymer induced by Ar^+ sputtering, which may make it more difficult to remove the PS. Finally, the PS was removed by an O_2 plasma treatment (250 W, 500 mTorr, 2 min).

3. Pt dots (130 nm) (35% geometrical Pt surface coverage) were placed on a ceria support (Figure 4d). The sample was made according to the following procedure: 20 nm ceria and 20 nm Pt films were sequentially evaporated on an oxidized Si wafer. PS particles (107 nm) (0.2 mM NaCl in the particle suspension) were adsorbed and partly melted on a hot plate at 112 °C for 1 min (to form flat Pt dots, Figure 4c). The sample was subsequently etched for 2.5 min (500 V, 0.2 mA/cm^2), and the PS was finally removed by an O_2 plasma treatment (250 W, 500 mTorr, 2 min).

Figure 9 shows the XPS spectra of the C1s region for samples from categories 1 and 2 above. The identical chemical composition (solid Pt films) of the samples makes them easy to compare quantitatively. The samples were analyzed as prepared and after oxidation in 19% O_2 at 400 °C for 30 min, in a pretreatment cell attached to the XPS apparatus, to remove carbon contamination deriving from the ambient. After the oxidation step, the pretreatment cell was pumped to vacuum and the samples were introduced into the XPS analysis chamber without being

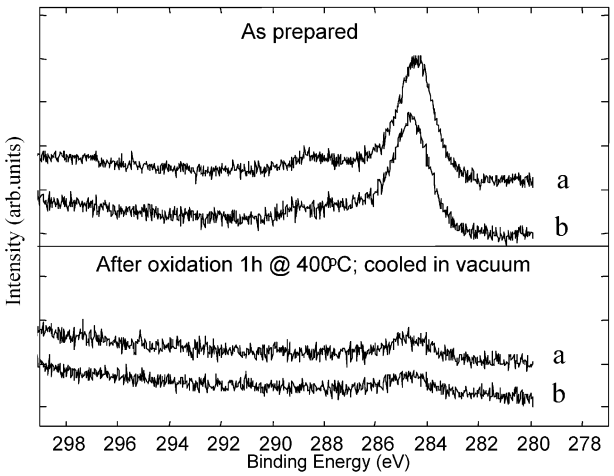

Figure 9. XPS spectra of the C1s region for (a) Pt film, which has been exposed to all the steps in the colloidal lithography process, and (b) reference Pt film. In the lower panel, the samples have been oxidized at 400 °C in 19% O_2 diluted in Ar for 1 h.

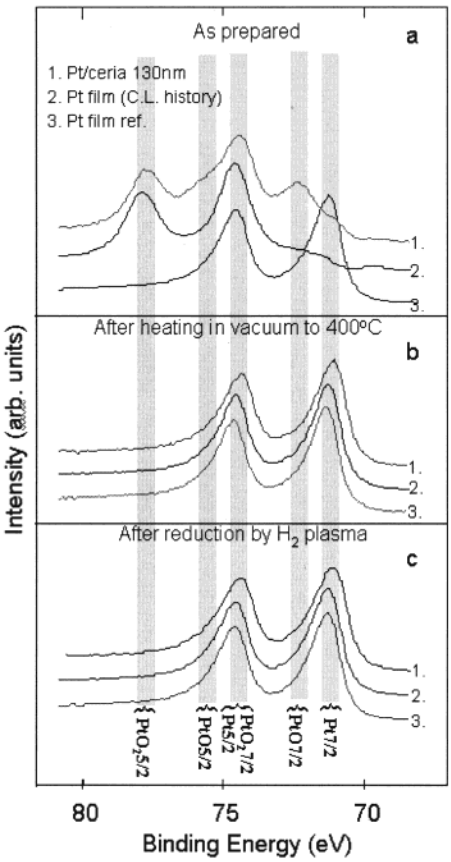

Figure 10. XPS spectra of the Pt4f region for a 130 nm Pt/ceria, a Pt film that has been exposed to all the steps in the colloidal lithography process, and an untreated Pt film as reference. The samples were analyzed (a) as prepared, (b) after heating in a vacuum to 400 °C and cooling to room temperature (5 K/min), and (c) after reduction by H_2 plasma (500 mTorr, 250 W, 2 min). The binding energies are internally calibrated to the C1s peak at 284.8 eV.

exposed to atmosphere. Analyzed as prepared, the sample exposed to the PS (category 1) showed the same amount of carbon as the Pt film reference (category 2), and after oxidation only traces (<1%) of carbon were left on both samples. This makes us draw the conclusion that the oxygen plasma treatment effectively removes all the PS. The XPS C1s spectrum from category 3 was not included in the analysis, since the ceria support may interact differently with carbon contamination than Pt.[14]

Figure 10 shows XPS spectra of the Pt4f region for samples from categories 1−3. Three samples from each category were analyzed: (i) one sample as prepared; (ii) one which was heated in a vacuum to 400 °C with a temperature ramp of 5 K/min, held at 400 °C for 2 min, and cooled and introduced into the XPS analysis chamber without being exposed to atmosphere; and finally, (iii) one sample reduced by H_2 plasma (250 W, 500 mTorr, 2 min). Table 1 shows the relative amounts of Pt, PtO, and PtO_2 obtained by deconvolution of the spectra using iterated Shirley background subtraction and Gauss−Lorentz peak fitting. On the basis of previous reports, the following constraints were made to quantify the spectra: (1) the separation between the 5/2 and 7/2 doublets of the Pt, PtO, and PtO_2 peaks were fixed to 3.30, 3.40, and 3.40 eV, respectively; the separation between Pt and PtO was fixed to 1.1 eV and the separation between Pt and PtO_2 to 2.0 eV; the area ratios between the Pt, PtO, and PtO_2 7/2:5/2 peaks were fixed to 1.30, 1.39, and 1.48, respectively.[37]

Table 1. Relative Amounts of Pt, PtO, and PtO_2 as Deduced from XPS

	Pt (%)	PtO(%)	PtO_2(%)
As Prepared			
130 nm Pt/ceria	5	33	61
Pt film (CL history)[a]	1	19	80
Pt film reference	71	28	1
After Heating in a Vacuum to 400 °C			
130 nm Pt/ceria	67	31	2
Pt film (CL history)	72	27	1
Pt film reference	71	28	1
After Reduction by H_2 Plasma[b]			
a-Pt/ceria 130 nm	67	31	2
b-Pt film (CL history)	69	30	1
c-Pt film reference	70	28	2

[a] The Pt film was exposed to all the steps in the colloidal lithography process (Figure 1). [b] Hydrogen plasma parameters: 250 W, 500 mTorr for 2 min.

From the results, it is evident that Pt becomes heavily oxidized during the fabrication process. New peaks appear at higher binding energies (above the $Pt4f_{5/2}$ peak, and between the $Pt4f_{7/2}$ and $Pt4f_{5/2}$ peaks), which correspond to PtO and PtO_2. The deep oxidation is a result of the O_2 plasma treatment.[38] Interestingly, the Pt film exposed to O_2 plasma exhibits a more oxidized Pt surface than the 130 nm Pt/ceria sample. Ceria is known to stabilize Pt oxides from being reduced to metallic Pt, but conversely it also appears to stabilize PtO from being oxidized to PtO_2. A simple in situ annealing step in connection with a catalytic activity measurement (Figure 10b) or an H_2 plasma treatment (Figure 10c) at the end of the fabrication process efficiently reduces Pt. The latter is in good agreement with the reported thermal stability of PtO_2.[38] The amount of PtO_x reported in Table 1 probably is influenced by chemisorbed O, which is expected to result in overestimation of the PtO contribution in our peak deconvolution procedure due to peak broadening. With reference to the data for the Pt film, which is known to be reduced to metallic Pt,[38] it is therefore reasonable to assume that the reduction steps transforms PtO_x to mainly Pt(0).

In circumstances where the O_2 plasma may be causing irreversible damage to the sample, care has to be taken. We have observed that Ru is removed from the sample by an O_2 plasma treatment similar to that described above. It appears that the O atoms volatilize Ru into gas-phase products. Preliminary results show that a milder way of removing the PS mask is to employ a UV/ozone treatment, that is, irradiation of the sample, kept in pure O_2 or air, with a UV lamp creating ozone. Another issue in this context is whether the oxygen plasma treatment causes redeposition of catalytic material on the support creating small (metal-containing) particles below the detection limit of SEM and AFM. The observation of metal volatilization in the case of Ru accentuates this issue. We have, however, not yet been able to confirm or reject this hypothesis. The difficulty in the exploration of this possible side effect lies in the necessary local chemical analysis of the surface area between the particles.

Samples from the three categories above were also analyzed regarding S and Cl contamination, since the PS particles contain sulfate groups, and NaCl was added to the particle suspension during the preparation of sample 3. No traces of these elements were detected in XPS.

(37) Kaushik, V. K. *Z. Phys. Chem.* **1991**, *173*, 105.
(38) Maya, L.; Riester, L.; Thundat, T.; Yust, C. S. *J. Appl. Phys.* **1998**, *84*, 6382.

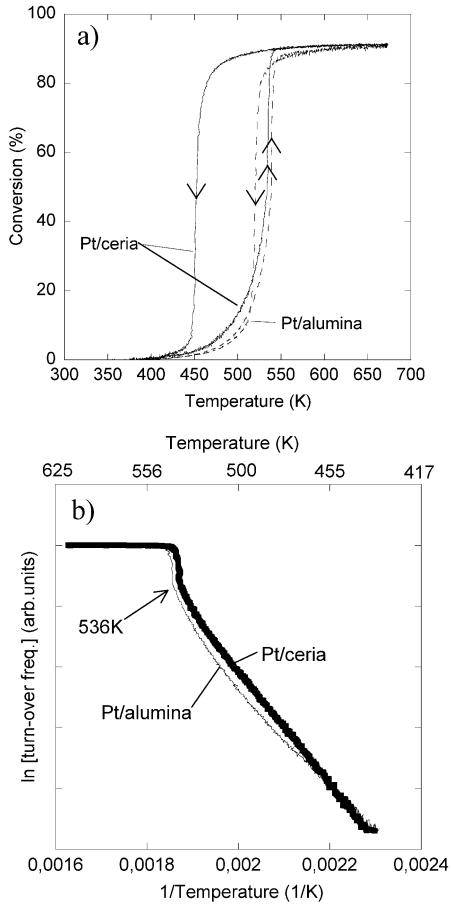

Figure 11. The CO conversion (a) and the corresponding Arrhenius plot (b) for a 130 nm Pt/ceria and Pt/alumina sample, respectively. The samples were heated (10 K/min) in a gas mixture of 0.3% CO and 1.2% O_2 to 673 K, held there for 2 min, and cooled at 10 K/min to 300 K. The samples were pretreated for 20 min in 5% O_2 and 20 min in 5% H_2 at 673 K, and the figures show the third CO oxidation cycle after the pretreatment. In (b), the point of catalytic ignition is indicated.

4. CO Oxidation

In this section, the CO oxidation characteristics at atmospheric pressures on Pt/alumina and Pt/ceria samples prepared by colloidal lithography are presented. Two sets of samples were prepared: (i) 130 nm flat Pt dots with 35% projected surface coverage on a 20 nm thick alumina film and (ii) 130 nm flat Pt dots with 35% projected surface coverage on a 20 nm thick ceria film. Variations of the alumina and ceria film thickness between 10 and 50 nm did not produce any differences regarding the CO oxidation characteristics. The thickness of the Pt dots was 14 nm for the Pt/alumina samples and 20 nm for the Pt/ceria samples. In Figure 4d, a SEM image of the 130 nm Pt/ceria sample is shown. The Pt/alumina sample looks essentially the same, except for a slightly lower height of the flat Pt dots. From analysis of the SEM images, we obtain a particle density of ca. 3×10^9 cm^{-2} and a nearest-neighbor distance of 194 nm (35% projected surface coverage) for both the Pt/ceria and Pt/alumina samples. A total of six samples were used in the CO oxidation measurements. No significant difference was observed between samples from the same batch.

4.1. Temperature Hysteresis and Catalytic Ignition. Figure 11a shows the CO to CO_2 conversion as a function of temperature obtained on Pt/alumina and the Pt/ceria and the corresponding Arrhenius plots. Both samples reached 92% conversion at $T > 600$ K and remained at this conversion up to 673 K. The apparent limited conversion is attributed to a slip of reactant molecules in the reactor, since at a flow of 30 cm^3/min the gas residence time is comparable to the gas mixing time in the reactor. During the temperature increase, both samples follow approximately the same trace, with a $T_{50,up} = 533$ K (T_{50} is defined as the temperature corresponding to 50% of the maximum conversion, that is, 46% absolute conversion in our case) for the Pt/ceria catalyst and $T_{50,up} = 538$ K for the Pt/alumina catalyst. During cooling (10 K/min), however, they distinctly diverge with $T_{50,down} = 452$ K for the Pt/ceria sample and $T_{50,down} = 521$ K for the Pt/alumina sample. The presence of a T-hysteresis can be expected for both samples from pure kinetic considerations taking into account the difference in adsorption kinetics of O_2 and CO and the rapid CO + O reaction.[6] However, since we are able to make samples with identical Pt coverage, sizes, and interparticle distance, irrespective of support material, we can unambiguously attribute the different T-hysteresis for Pt/ceria and Pt/alumina to the well-known oxygen storage capacity of ceria,[14] which provides an additional oxygen source that prevents CO poisoning due to a spillover mechanism between ceria and Pt.[10,40]

From a fundamental point of view, it is important to know exactly at what temperature the transition from a kinetically controlled regime to a mass transport limited regime occurs as a function of reactant composition, particle dimensions, support type, and so forth. It is also important if one wants to determine kinetic parameters for the catalytic surface process under consideration. A typical conversion curve may be a smooth transition when going from a kinetically controlled to a mass transport controlled regime. This is the so-called "light-off" situation and results in a sigmoidal form of the conversion curve. This is the case if the heat generated by the catalytic reaction and the external heating ($Q_{in} = Q_r + Q_{ext}$) is smaller than the heat losses of the system (Q_{loss}), $dQ_{in}/dT < dQ_{loss}/dT$.[41] The conversion curve may also rapidly increase at a certain temperature. This is the case when at a certain temperature $dQ_{in}/dT > dQ_{loss}/dT$, which leads to a self-accelerated process where the CO_2 production (giving rise to reaction heat and free sites) and the T-rise (increasing the rate of CO_2 conversion nonlinearly) amplify each other.[42,43] In the experiments shown in Figure 11a (using 0.3% CO in the gas mixture), we were not able to observe any T-rise (when going up in temperature) with our temperature probe. To determine if, and at what temperature, catalytic ignition occurred, we instead devised the following scheme: A 130 nm Pt/ceria sample was heated stepwise in small steps with constant external power in a CO oxidation mixture of 5% CO + 20% O_2 (i.e., the same gas mixing ratio but with 16 times higher CO concentration, thus boosting the chemical energy input). In Figure 12, it is seen that at 608 K a sudden increase in the temperature occurs, along with a simultaneous rise in the CO_2 production, which proves catalytic ignition takes place at 608 K in this particular gas mixture. The Arrhenius plot obtained from the latter experiment exhibits a step at the ignition point. This is because the local temperature on the Pt particles increases much more than what we measure with our temperature probe at the

(39) Österlund, L.; Kielbassa, S.; Werdinius, C.; Kasemo, B. *J. Catal.*, in press.
(40) Zhdanov, V. P.; Kasemo, B. *Appl. Surf. Sci.* **1998**, *135*, 297.
(41) Frank-Kamenetskii, D. A. *Diffusion and heat transfer in chemical kinetics*, 2nd ed.; Plenum: New York, 1969.
(42) Rinnemo, M.; Kulginov, D.; Johansson, S.; Wong, K. L.; Zhdanov, V. P.; Kasemo, B. *Surf. Sci.* **1997**, *376*, 297.
(43) Dicke, J.; Rotermund, H. H.; Lauterbach, J. *Surf. Sci.* **2000**, *454*, 352.

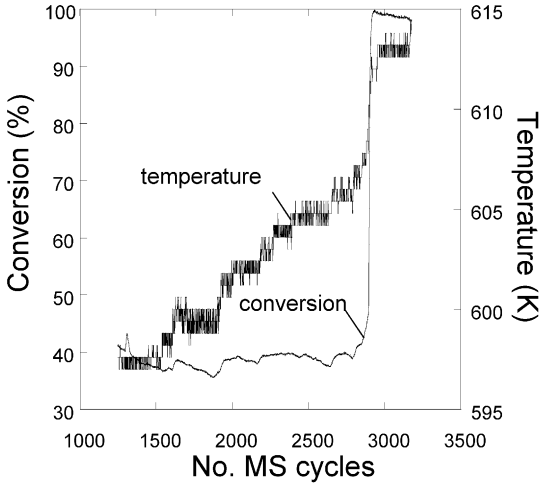

Figure 12. The measured CO conversion and sample temperature as a function of time (∝cycle number) obtained when stepwise increasing the heating power in steps of 2 K in a gas mixture of 5% CO in 20% O_2. The dwell time between each temperature increase was about 300 s (1 cycle ~ 1 s).

ignition point. A corresponding step in the Arrhenius plot (when going up in temperature) is also evident at lower CO concentrations, where no *T*-rise was observed (Figure 11b). This indirectly shows that catalytic ignition also occurs at lower CO concentrations. A precise determination of the kinetically controlled regime provides important input in the analysis of the CO oxidation, which we will make use of below.

4.2. Catalyst Activation and Effects of Pretreatment. A catalyst must be "activated" prior to experiments to remove residual contamination from the preparation procedure and hydrocarbons from ambient air exposures. Such activations normally include an oxidation step followed by a reduction step. Characterization of as-prepared Pt/alumina and Pt/ceria model catalysts was therefore studied as a function of pretreatment. All samples were pretreated in the reactors (i.e., they were not prereduced by H_2 plasma).

Figures 13A and 14A show a few representative conversion curves for the initial CO oxidation cycles on 130 nm Pt/ceria and Pt/alumina, respectively. The experiments are divided into three regimes: In the first regime, the CO oxidation is measured on a fresh catalyst without any pretreatments. In the second regime, the samples were oxidized and reduced prior to the CO oxidation experiments (5% O_2/Ar for 20 min followed by 5%H_2/Ar for 20 min at 673 K). Finally, in the third regime, the samples were oxidized prior to the CO oxidation cycles (5% O_2/Ar for 20 min at 673 K). In Figures 13B and 14B, $T_{50,up}$, $T_{50,down}$, and the apparent activation energy, E_a^*, are shown, using the procedure outlined above to determine the kinetically controlled regime. The latter is, however, not the activation energy of the CO + O Langmuir−Hinshelwood step, since the CO oxidation reaction on Pt is a coupled reaction involving complex surface reactions (and possibly also Pt oxidation[10,43]), where in particular the O_2 adsorption is inefficient.[10,41] Moreover, the measurements are not steady-state measurements. However, the relative magnitudes of E_a^* can be used to compare identically performed CO oxidation measurements and contain information on the shapes of the conversion curves, which complement the T_{50} values. For these reasons, we have chosen to label E_a^* in arbitrary units. In Figure 13B, we see that T_{50} (up and down) and E_a^* initially shift down on Pt/ceria. The *T*-hysteresis is ca. 100 K and becomes

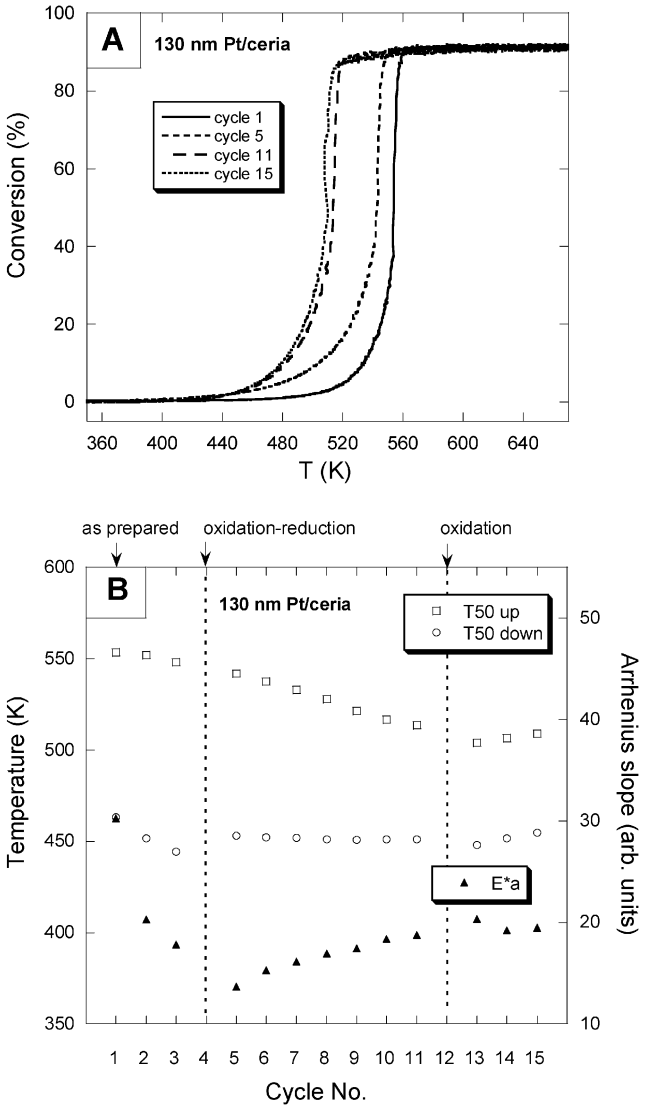

Figure 13. (A) Selected CO conversion curves (0.3% CO and 1.2% O_2) obtained on a fresh 130 nm Pt/ceria catalyst corresponding to the cycle numbers indicated in (B). (B) T_{50} and E_a^* values obtained from several subsequent CO oxidation cycles.

more pronounced after a few CO oxidation cycles, which may be attributed to a cleanup and reduction of the oxidized catalyst. After a subsequent oxidation and reduction treatment, the $T_{50,up}$ gradually shifts down, and simultaneously the *T*-hysteresis window shrinks and E_a^* continuously increases with every CO oxidation cycle. An additional oxidation treatment at 673 K does not affect the T_{50} and E_a^* significantly. In Figure 14B, the corresponding results for 130 nm Pt/alumina are shown. The T_{50} and E_a^* initially shift down. In contrast to Pt/ceria, there is an upshift in T_{50} and E_a^* following either an oxidation−reduction or an oxidation treatment. The absolute value of E_a^* is in all cases similar to that of Pt/ceria. After >10 cycles, there are no significant changes in the conversion curves following repeated CO oxidation experiments. A qualitative XPS analysis of the Pt/alumina sample indicates that the Pt is mainly in the reduced state and the chemical state does not change significantly after additional CO oxidation cycles. There is no evidence for stabilization of PtO on the Pt/alumina sample, as seen on the Pt/ceria sample (Figure 10). (A quantitative XPS analysis of Pt/alumina is complicated by the overlap of the Al2p and Pt4f peaks.) We note in Figure 14A that there is a tendency that the conversion decreases versus

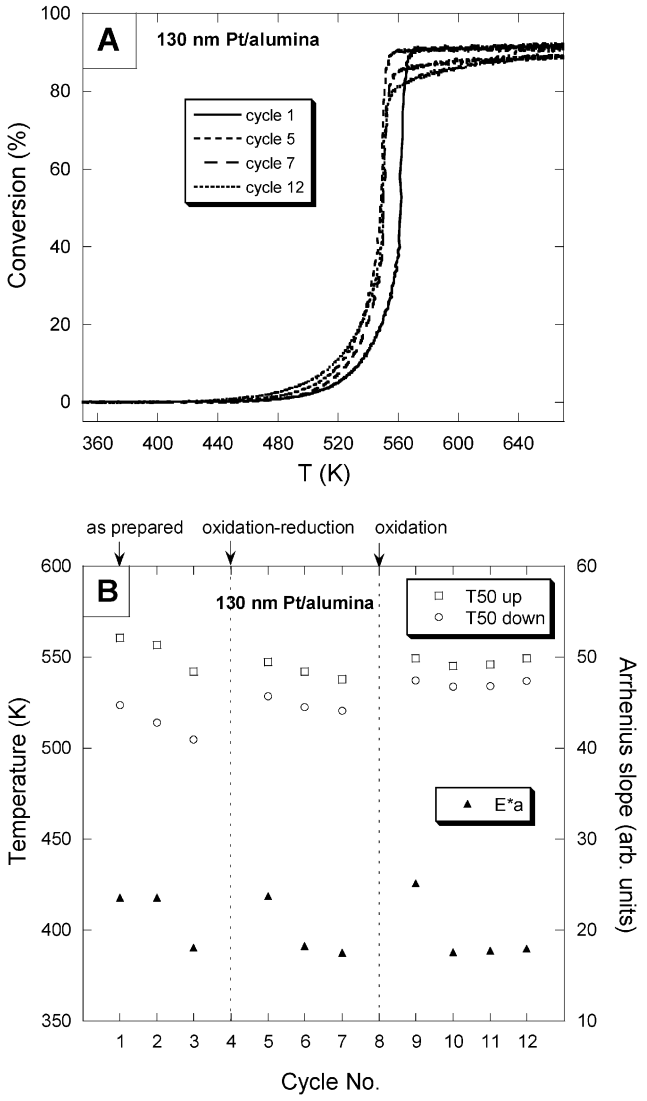

Figure 14. (A) Selected CO conversion curves (0.3% CO and 1.2% O_2) obtained on a fresh 130 nm Pt/alumina catalyst corresponding to the cycle numbers indicated in (B). (B) T_{50} and E^*_a values obtained from several subsequent CO oxidation cycles.

cycle number just after the ignition point. At present, we do not have an explanation for this latter phenomenon, but it is also shown to occur for samples from different batches and with different particle sizes. However, the overall results from the CO oxidation measurements on the Pt/alumina and Pt/ceria model catalysts are in good agreement with previous studies on wet-impregnated catalysts.[44−46] Ceria is shown to promote the low-temperature reactivity, which is manifested in a lower $T_{50,up}$ (ca. 50 K) and a broader *T*-hysteresis. Both observations can be explained by the well-known oxygen storage capacity of ceria and/or interfacial Pt−Ce−O species formation,[10,40,47,48] which is also in agreement with the observed stabilization of a PtO species in the case of Pt/ceria seen in XPS.

5. Conclusions

We have demonstrated the principles of colloidal lithography to prepare well-defined Pt/ceria and Pt/alumina model catalysts (both 2D and 3D structures). The Pt particles become heavily oxidized (Pt/ceria is observed to stabilize $Pt^{II}O$ formation) after the O_2 plasma cleaning step employed here to remove the polystyrene particle mask, but they can readily be reduced either by hydrogen plasma or annealing. No traces of contamination are apparent after fabrication. A CO oxidation experiment on Pt/alumina and Pt/ceria model catalysts shows general good agreement with literature data and demonstrates the possibility to characterize in detail a catalytic reaction by the colloidal lithography method. Here the results of the catalytic ignition phenomenon and the influence of support material were presented (demonstrating the well-known oxygen storage capacity of ceria). In this study, fairly large nanoparticles were used to facilitate an iterative SEM structural analysis, but scale-down to <10 nm should be straightforward. Because of the versatility of the colloidal lithography technique and the fast parallel way samples can be made, the method is appropriate to rapidly screen interesting materials and structure combinations, while still having precise control of the chemical and structural properties of the catalysts.

Acknowledgment. Dr. Duncan Sutherland and Per Hanarp are greatly acknowledged for sharing their knowledge about the colloidal lithography process. The work in this paper was performed within the Competence Centre for Catalysis, which is financially supported by the Swedish National Energy Administration and the member companies: AB Volvo, Johnson Matthey-CSD, Saab Automobile AB, Perstorp AB, MTC AB, Eka Chemicals, and the Swedish Space Corporation.

Note Added after ASAP Posting. This article was released ASAP on 11/23/2002. Changes made after posting were as follows: section 3.1. Process Description, first paragraph, second sentence, (Figure 1, step I) was changed to (Figure 1, steps I and II) and (Figure 1, step II) was changed to (Figure 1, step III); Figure 1 caption was modified to identify the left panel; section 3.1. Process Description, last paragraph, second sentence, O_2 plasma was deleted; sections 3.3 and 3.4 were transposed and relabeled; section 3.4. Particle Size, last paragraph, first sentence, alumina was changed to silica; section 3.7. Removal of the Polystyrene Template Particles, second sentence O_2 treated with changed to O_2 plasma treated; section 3.7. Removal of the Polystyrene Template Particles, paragraph 7, sixth sentence, Figure 11b is changed to Figure 10b and Figure 11c is changed to Figure 10c; section 3.7. Removal of the Polystyrene Template Particles, paragraph 9, first sentence, the Cl and S were rearranged to S and Cl; section 4. CO Oxidation, first paragraph, second sentence, the sentence was modified; the caption to Figure 13 was modified; section 4.2. Catalyst Activation and Effects of Pretreatment, second paragraph, end of sixth sentence, value was changed to values; the caption to Figure 14 was modified; section 4.2. Catalyst Activation and Effects of Pretreatment, second paragraph, the 17th and 18th sentence were modifed; Figure 10 was revised, it is now more clearly labeled. The correct version was posted on 12/12/2002.

LA026459J

(44) Zafiris, G. S.; Gorte, R. J. *J. Catal.* **1993**, *143*, 86.
(45) Törncrona, A.; Skoglundh, M.; Thormählen, P.; Fridell, E.; Jobson, E. *Appl. Catal., B* **1997**, *14*, 131.
(46) Serre, C.; Garin, F.; Belot, G.; Maire, G. *J. Catal.* **1993**, *141*, 9.
(47) Bernal, S. *Catal. Today* **1999**, *50*, 175.
(48) Bunluesiin, T.; Putna, E. S.; Gorte, R. *J. Catal. Lett.* **1996**, *41*, 1.